

## Article

# Nano-Iron Oxide Coating for Enhanced Heat Transfer in Gas–Solid Fluidized Bed Systems

Fadhl H. Faraj <sup>1</sup>, Jamal M. Ali <sup>1,\*</sup> , Sarmad T. Najim <sup>2</sup>, Abbas J. Sultan <sup>1,3,\*</sup> , Saja M. Alardhi <sup>4</sup> and Hasan Sh. Majdi <sup>5</sup>

<sup>1</sup> Chemical Engineering Department, University of Technology-Iraq, Baghdad 10066, Iraq; fadhl.h.faraj@uotechnology.edu.iq

<sup>2</sup> Chemical Engineering Department, Al-Nahrain University, Baghdad 10072, Iraq; sarmad.t.najim@nahrainuniv.edu.iq

<sup>3</sup> Department of Chemical and Biochemical Engineering, Missouri University of Science and Technology, Rolla, MO 65409-1230, USA

<sup>4</sup> Nanotechnology and Advanced Material Research Center, University of Technology-Iraq, Baghdad 10066, Iraq; 11659@uotechnology.edu.iq

<sup>5</sup> Chemical Engineering and Petroleum Industries Department, Al-Mustaqbal University, Hillah 51001, Iraq; dr.hasanshker@uomus.edu.iq

\* Correspondence: jamal.m.ali@uotechnology.edu.iq (J.M.A.); abbas.j.sultan@uotechnology.edu.iq (A.J.S.)

**Abstract:** This study explores using iron oxide coatings on glass beads to improve heat transfer efficiency in fluidized bed reactors. Techniques such as BET surface area analysis, SEM imaging, and X-ray diffraction were used to characterize the coated beads. Results showed the successful creation of a crystalline iron layer on the beads' surface and increased thermal conductivity, especially at elevated temperatures. The study also quantified the impact of air surface velocity and heating power on the heat transfer coefficient, revealing substantial improvements, especially at higher velocities. It was found that the heat transfer coefficient for 600  $\mu\text{m}$  glass beads increases significantly from 336.4  $\text{W}/\text{m}^2\cdot\text{K}$  to 390.3  $\text{W}/\text{m}^2\cdot\text{K}$  when the velocity is 0.27  $\text{m}/\text{s}$  and the heating flux is 125  $\text{W}$ . This demonstrates the effectiveness of the iron oxide coating in improving heat transfer. The results of this study emphasize the efficacy of iron oxide coatings in augmenting heat transmission characteristics, particularly in fluidized bed reactor.



**Citation:** Faraj, F.H.; Ali, J.M.; Najim, S.T.; Sultan, A.J.; Alardhi, S.M.; Majdi, H.S. Nano-Iron Oxide Coating for Enhanced Heat Transfer in Gas–Solid Fluidized Bed Systems.

*ChemEngineering* **2024**, *8*, 9.  
<https://doi.org/10.3390/chemengineering8010009>

Academic Editor: Vincenzo Russo

Received: 4 October 2023

Revised: 29 November 2023

Accepted: 14 December 2023

Published: 2 January 2024



**Copyright:** © 2024 by the authors. Licensee MDPI, Basel, Switzerland. This article is an open access article distributed under the terms and conditions of the Creative Commons Attribution (CC BY) license (<https://creativecommons.org/licenses/by/4.0/>).

**Keywords:** nano-iron oxide coating; heat transfer enhancement; fluidized bed reactors; coating characterization; computational fluid dynamics

## 1. Introduction

Fluidized bed reactors have become widely recognized and essential in various industrial applications. The reactors under consideration, distinguished by solid particles suspended in a gaseous medium, have garnered significant attention due to their distinct benefits in various applications, from petrochemical processing to producing renewable energy [1–3]. Fluidized beds are widely recognized for their exceptional mixing properties, remarkable heat transfer capabilities, and improved mass transfer rates [4,5]. These characteristics render fluidized beds indispensable in various industrial processes, contributing significantly to their efficiency and sustainability.

The performance and overall efficiency of these reactors are influenced by the efficient heat transfer between a gas phase and solid particles, which is an essential process [6–8]. Improving heat transfer within these systems has been a persistent and significant obstacle, directly influencing energy consumption, product quality, and environmental sustainability.

Numerous scholars have investigated the diverse facets of heat transfer in fluidized beds, enhancing our comprehension of the intricate phenomena inherent in this mechanism and devising more effective and environmentally friendly technologies for applications encompassing combustion, chemical reactions, and particle drying [9–15]. The most recent

experimental research has shown robust findings regarding the augmentation of heat transport in fluidized bed reactors [16–18]. Earlier investigations have primarily focused on modifying reactor configurations, improving gas distribution, and implementing surface treatments to enhance heat transfer rates.

In recent years, nanotechnology has emerged as an up-and-coming option for augmenting heat transfer capabilities inside fluidized bed systems. Using nano-iron oxide coatings offers a novel method to enhance thermal conductivity and optimize heat exchange efficiency. Nanostructured materials have distinct characteristics that distinguish them from ordinary materials [19,20]. These include a high surface area-to-volume ratio and improved thermal conductivity. These distinctive features make them highly promising for overcoming the longstanding limits associated with conventional fluidized bed heat transfer processes [21–24]. A growing body of work emphasizes the significance of coatings in improving heat transfer. The use of thin-film coatings, for instance, can lead to more efficient heat transfer and better control over process conditions. Additionally, coatings can change the surface morphology, offering a larger surface area for convective heat transfer [25–27]. Although previous research has investigated multiple parameters influencing heat transmission in fluidized beds, more particular studies need to examine the impact of particle coatings, such as iron oxide, on enhancing heat transfer capabilities. Most previous research has focused on naturally occurring materials, such as sand particles or conventional metals, with little investigation into coated or manufactured materials. Moreover, numerous studies have imposed restrictions on their operational parameters, restricting the extent to which their conclusions can be generalized. The complicated and multifaceted characteristics of heat transmission in fluidized bed systems necessitate a more comprehensive understanding, encompassing the potential impact of various coatings and a broader spectrum of operational parameters on the resulting outcomes.

The objective of this study was first to explore the impact of applying iron oxide coatings to glass beads on the heat transfer process within a fluidized bed reactor. The primary premise posits that applying these coatings can substantially boost the heat transfer rates inside the given system. Extensive tests were conducted to provide empirical support for this concept, wherein operational parameters such as air velocities, particle size, and heating capacities were systematically varied.

The study makes multiple additions that address the existing literature body's current shortage. This study presents iron oxide as a new coating material for particles in a fluidized bed, broadening the range of materials to enhance heat transfer processes. Furthermore, the research employs a complete experimental design encompassing various operational factors, such as different air velocities and heating capabilities. This approach allows for a more nuanced comprehension of the subject matter, surpassing the constraints of previous studies. These findings have significant implications for improving energy efficiency, decreasing operational expenses, and strengthening process control within industrial settings.

## 2. Experimental Work

The experimental work in this study aimed to investigate and enhance heat transfer within fluidized bed reactors. This section provides an overview of the materials employed, the procedure for coating glass beads with iron oxides, and an in-depth description of the experimental configuration.

### 2.1. Materials

The present experimental investigation employed glass beads obtained from Zhengzhou Xinli Wear Resistant Material Co., Ltd. (Zhengzhou, China), demonstrating distinct compositional and physical characteristics. The glass beads are composed of multiple components specified in Table 1. Furthermore, Table 2 displays the overall physical characteristics obtained from analyzing the glass beads. The selection of spherical glass beads is consistent with known methodologies in fluidized bed research, hence, improving

the dependability and comparability of our results with the pre-existing body of knowledge in this domain.

**Table 1.** Chemical composition of glass beads.

Component	Value
SiO <sub>2</sub>	72.00–73.00%
Na <sub>2</sub> O	13.30–14.30%
CaO	7.20–9.20%
MgTiO	3.50–4.00%
Al <sub>2</sub> O <sub>3</sub>	0.80–2.00%
K <sub>2</sub> O	0.20–0.60%
SO <sub>3</sub>	0.20–0.30%

**Table 2.** Typical physical properties of glass beads.

Typical Physical Properties	Value
Grain shape	Round
Melting point	1200 °C
Specific gravity	2.50
Bulk density	2.5 g/cm <sup>3</sup>
Voidage	0.45

In this investigation, the purposeful selection of two distinct sizes of glass beads, namely 200 and 600  $\mu\text{m}$ , is to quantify the influence of bead size on the heat transfer coefficient. By conducting a comparative analysis of the outcomes derived from these two different sizes, one can gain insights into the impact of glass bead size on the efficiency of the heat transfer inside the fluidized bed system. Nevertheless, it is crucial to acknowledge that utilizing only two distinct sizes of glass beads may not comprehensively capture the intricacies inherent in real-life scenarios. Therefore, in real-world scenarios, a distribution of particle sizes is expected to be encountered, which might have varying effects on heat transmission properties. The rationale behind selecting two distinct sizes of glass beads was likely driven by improving the dependability and comparability of the findings to the current body of knowledge within the respective discipline. In order to conduct a more comprehensive investigation of the impact of bead size distribution on heat transfer performance, it is recommended that future studies incorporate a broader spectrum of bead sizes. This would facilitate a more comprehensive understanding of the influence of various size distributions on heat transfer rates in fluidized bed systems.

## 2.2. Experimental Methodology: Application of Iron Oxide Coating onto Glass Beads

Iron oxide thin-film coatings are crucial in augmenting thermal conductivity and enabling heat transfer in various applications [28]. These coatings exhibit a high level of thermal conductivity, thereby facilitating the dissipation of heat and, thus, improving the operational efficiency of diverse devices and heat exchangers. Moreover, they exhibit high thermoelectric efficiency, successfully transforming surplus thermal energy into electrical power, thereby making them indispensable in various industrial sectors and technological applications. The experimental methodology consists of the following steps.

### 2.2.1. Preparation of Glass Beads

The first stage in the experimental protocol entailed careful and thorough preparation of the glass beads. In order to establish an optimal surface for the subsequent coating procedure, the glass beads underwent a complete cleaning process with a suitable solvent, specifically ethanol. The primary objective of this cleaning procedure was to remove any superficial impurities that could hinder the subsequent coating process. Following this, the glass beads underwent a thorough drying process to guarantee the total elimination of any remaining solvent residues.

### 2.2.2. Synthesis of Iron Oxide Precursor Solution

In order to commence the process of iron oxide coating, a solution of iron (II) sulfate, an iron salt, was dissolved in deionized water. The dissolution process utilized a ratio of 18 g of iron salt per 1 kg of glass beads, forming a transparent solution. The iron salt concentration in the solution was adjusted to correspond with the intended thickness and characteristics of the resulting iron oxide layer [29].

### 2.2.3. Iron Oxide Precipitation

The process of iron oxide coating production was achieved using the precipitation method. The addition of sodium hydroxide to the iron salt solution was performed carefully and gradually, with each drop added sparingly. Throughout the process, continuous stirring was maintained. The pH of the solution was carefully monitored and controlled within the critical range of 8–10 to facilitate the successful synthesis of iron oxide nanoparticles [30].

### 2.2.4. Glass Bead Coating

Following this, the glass beads that had been cleaned were submerged in a suspension of precipitated iron oxide, ensuring that the stirring process was continuous to achieve a coating on the glass beads that was both uniform and consistent.

### 2.2.5. Drying of Coated Beads

After the practical application of the coating, the glass beads were meticulously extracted from the suspension and introduced to the drying procedure. The drying process consisted of placing the glass beads coated with the substance in an oven set at 70 °C for 48 h.

The experimental approach employed in this study was undertaken with great attention to detail, ensuring the successful coating of glass beads with iron oxide. This coating process has been found to significantly improve the thermal conductivity of the beads, opening up several possibilities for use in heat transfer processes.

## 2.3. Description of the Experimental Setup

The experimental equipment selected for the research of heat transfer processes was a gas–solid fluidized bed column. The experimental arrangement included glass beads of two sizes, specifically 200  $\mu\text{m}$  and 600  $\mu\text{m}$ , to create a fixed bed measuring 30 cm in height before the fluidization process. The fluidizing column was fabricated using Perspex material, including an inner diameter of 10 cm and a height of 2 m. A perforated plate was employed in the column to serve as an air distributor. During experiments, various superficial air velocities were utilized, ranging from 0.1 to 0.5 m/s for both glass bead sizes.

The study addressed numerous crucial areas, namely the positioning of the heating element, the exploration of the local heat transfer coefficient, and an analysis of gas flow dynamics. The main aim of this study was to experimentally determine the overall heat transfer coefficient in a gas–solid fluidized bed system, with a systematic variation of important parameters, including heat fluxes and gas flow rates.

In order to enable regulated heating, a vertically positioned electrical heater was built within the fluidizing column. The heater had a diameter of 20 mm and a length of 300 mm. Various power supplies, ranging from 50 to 125 watts, were utilized to attain the appropriate experimental conditions. Figure 1 includes a schematic diagram of the experimental setup for reference.

The gas distributor was designed with a perforated plate and a triangular arrangement, considering the principles of orifice theory. The distributor consisted of 52 orifices, each measuring 2 mm in diameter. The researchers determined that the proportion of unobstructed space within the distributor plate was 1.7% [31].

In order to provide precise and reliable temperature measurements, a total of seven Type K thermocouples were carefully calibrated and afterward incorporated into the experimental configuration. The thermocouple was initially placed in the inlet part of

the fluidized bed column, precisely positioned 10 cm below the distributor, to monitor the temperature of the incoming gas. The second thermocouple was placed 10 cm above the distributor to measure the temperature of the bed accurately. The five remaining sensors were uniformly distributed in the vertical plane above the second thermocouple.

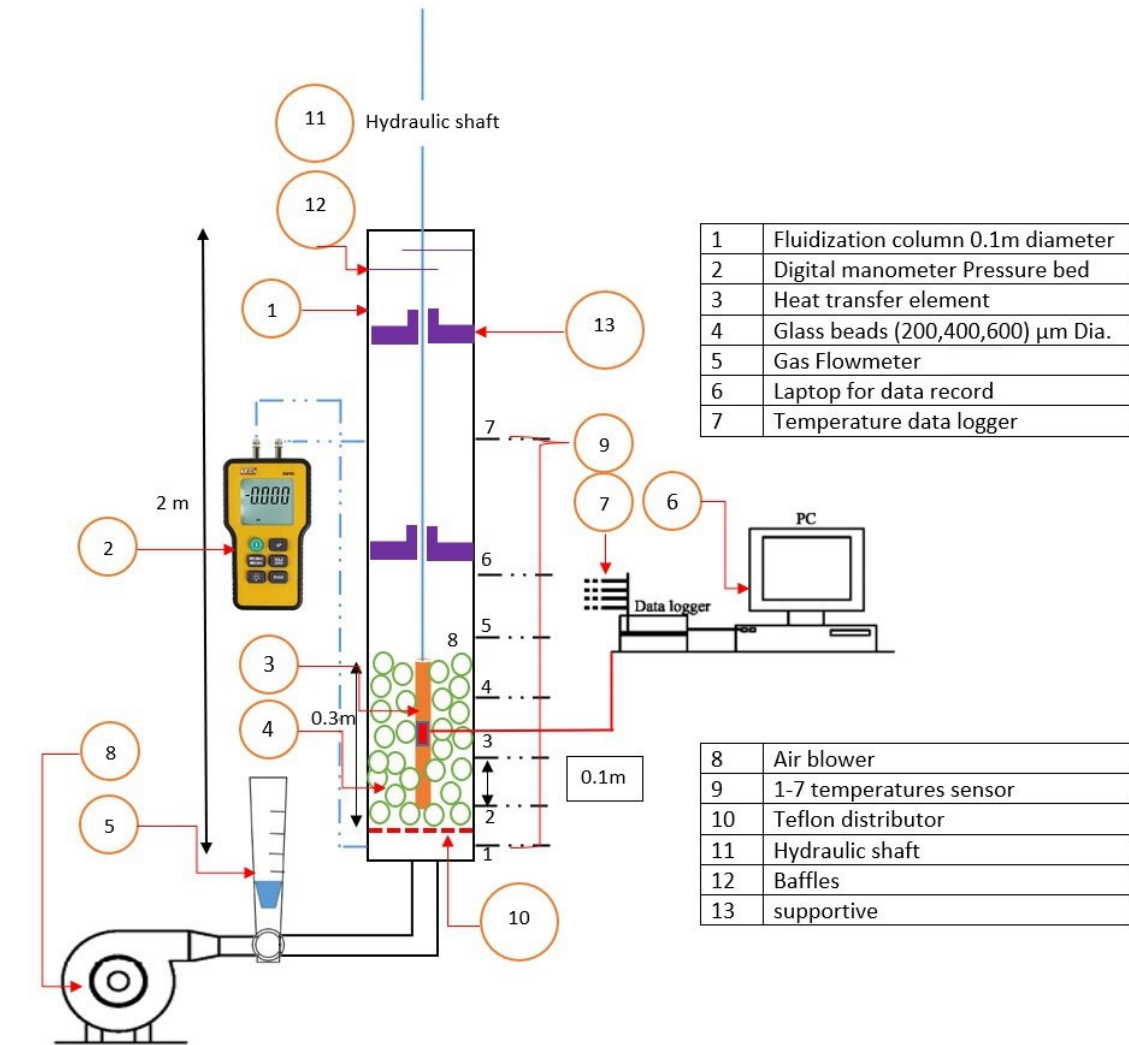


**Figure 1.** Schematic diagram of the experimental apparatus.

A manometer manufactured by Shenzhen Yowexa Measurement Technology Co., Ltd. (Guangdong, China) was employed to evaluate fluctuations in pressure within the fluidized bed. This manometer featured two pressure positions and a 5/16-inch-diameter pressure port, allowing precise pressure drop measurements along the fluidized bed. Moreover, the Werie Rietschle SKG 270-2.02 (PAGUS company, Leipzig, Germany), an air blower, served as a regenerative vacuum blower, exhibiting the ability to produce negative pressure or vacuum for many industrial purposes. The air blower exhibited a power rating of 2.6 kilowatts, a pressure range of 22 pounds per square inch, and a maximum flow rate of 150 cubic meters per hour (equivalent to 88.28 cubic feet per minute).

It is important to mention that the glass beads were in thermal equilibrium with the air. This was guaranteed by allowing sufficient time for the glass beads to reach the same temperature as the surrounding air before conducting the experiments.

The local heat transfer coefficient along the probe was estimated from the equation:

$$h_i = \frac{q}{A_S \Delta T} = \frac{VI}{A_S(T_{Si} - T_{bi})} \quad (1)$$

where the equation relates the heat transfer coefficient ( $h_i$ ) at a specific interface or surface to the heat transfer rate ( $q$ ) through that interface. It takes into account the applied voltage ( $V$ ) and current ( $I$ ) passing through the interface, as well as the cross-sectional area ( $A_S$ ) and the temperature difference ( $T_{si} - T_{bi}$ ) between the surface temperature ( $T_{si}$ ) and the bulk temperature ( $T_{bi}$ ) of the material. The average heat transfer coefficient was estimated from the local heat transfer coefficients:

$$h_{avg.} = \frac{h_1 + h_2 + h_3 + \dots + h_i}{i} \quad (2)$$

However, before the results were presented, the uncertainty analysis was investigated for its potential to influence the accuracy of the data. The superficial gas velocity was found to have an uncertainty of about 1.5%, mainly due to an error in instrumental precision (manometer) provided by the manufacturing company.

### 3. Results and Discussion

#### 3.1. Nano Coating Characterization

The coated glass beads were characterized with different tests, as listed below.

##### 3.1.1. Bet Surface Area Analysis

The BET (Brunauer–Emmett–Teller) method was utilized to ascertain the surface area of the glass beads both before and after applying a coating. The glass beads demonstrated a surface area of 1.3801 m<sup>2</sup>/g before applying a coating. Once the coating procedure was performed, there was a substantial increase in the surface area, reaching a value of 3.0511 m<sup>2</sup>/g. The observed rise in the measured quantity can be ascribed to the existence of a crystalline iron layer on the surface of the glass bead. Additional findings can be validated by conducting X-ray diffraction (XRD) research and scanning electron microscope (SEM) imaging.

##### 3.1.2. Scanning Electron Microscopy (SEM) Analysis

Scanning electron microscopy (SEM) analysis is of the utmost importance in material characterization, as it enables the acquisition of high-resolution surface images. The bead characterization procedure is significantly influenced by its role. Scanning electron microscopy provides valuable insights into multiple facets of the glass beads, encompassing their dimensions, shape, size, and surface morphology. We employed SEM to evaluate both uncoated and coated glass beads. Before applying a coating, uncoated glass beads generally display a very level surface with minor flaws, including little protrusions and abrasions caused by the inherent irregularity of the glass material.

Following the completion of the coating procedure, SEM pictures exhibit the apparent changes. The formation of iron oxide coatings on the surface of the beads can result in the development of either a continuous or granular layer, which is contingent upon factors such as thickness and uniformity. Pictures taken with an SEM are used as diagnostic tools to check the uniformity of the coating and identify any problems, such as areas that are not appropriately covered.

Additionally, it is essential to acknowledge that the diameter of the iron oxide crystals, as depicted in Figure 2, was acquired through image analysis software during the SEM study. After the magnification was increased to 200 nm, the iron oxide crystals were seen to have an average diameter of 27 nm. Nevertheless, it is crucial to recognize that the glass beads themselves display discrepancies in their sizes, a matter that will be further discussed in later examinations.

SEM pictures before and after coating are depicted in Figure 2. The images were captured at a magnification of 500 nm to observe the nanoscale surface morphological alterations. The SEM image before coating exhibits a predominantly clean surface, with slight imperfections, bumps, and scratches attributable to the natural unevenness of the original glass bead surface.

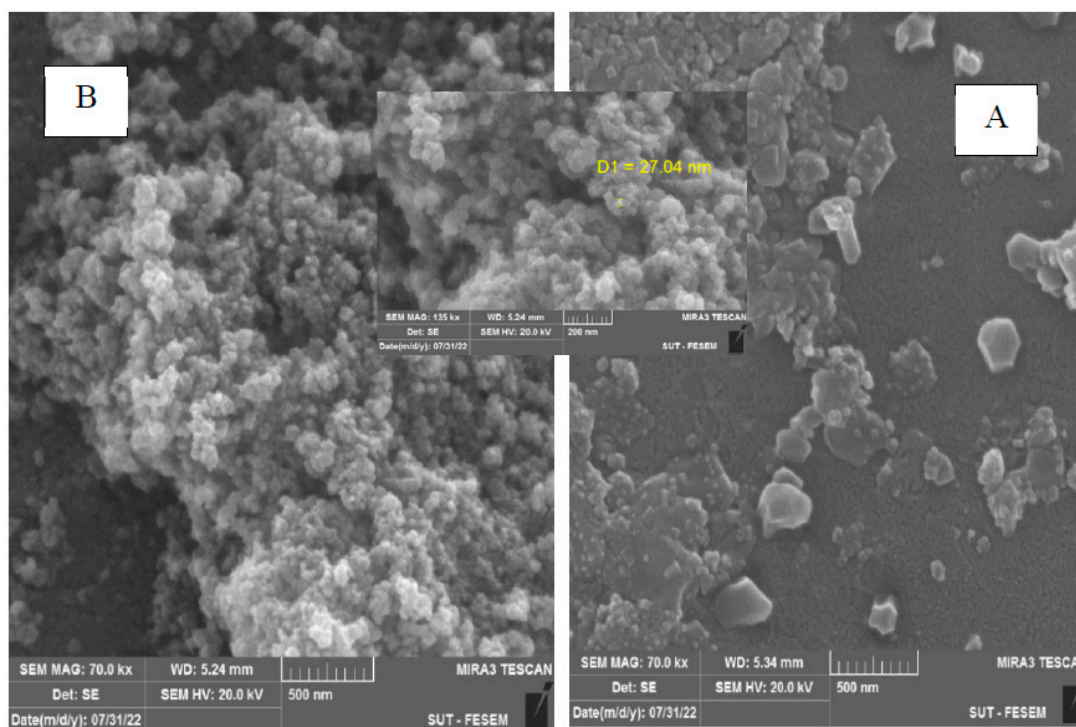


**Figure 2.** SEM images of samples (A) before and (B) after coating.

Following the completion of the coating procedure, the SEM pictures, depicted in Figure 2, exhibit the discernible existence of iron oxide crystalline formations on the surface of the glass beads. Upon further magnification at 200 nm, it is observed that the iron oxide crystals possess a diameter of 27 nm. The enlarged surface area of the coated glass beads is attributed to the small size, high density, and extensive distribution of the iron crystals. The morphology of the coating, or physical structure, is a crucial factor that significantly impacts thermal conductivity in a fluidized bed system. The potential for significantly enhancing heat transfer efficiency lies in using a thinner coating with a higher thermal conductivity than the substrate. The homogeneity of the coating is equally essential. Non-uniform coverage may lead to regions characterized by different thermal conductivities, resulting in an uneven heat distribution and a reduction in the overall efficiency of the system.

Moreover, it is important to acknowledge that smooth and rough surfaces can affect heat conductivity. A smooth surface can increase the contact area between the fluid and the surface, enhancing heat transmission. Conversely, a rough or porous surface can retain small amounts of fluid, which could further enhance heat transfer. Moreover, materials that possess higher levels of crystallinity inherently demonstrate enhanced thermal conductivities due to the efficient transmission of heat through their well-organized lattice structures. Therefore, it can be determined that the iron oxide coating on the glass beads has a crystalline structure, as confirmed through X-ray diffraction (XRD) research.

### 3.1.3. X-ray Diffraction (XRD)

X-ray diffraction (XRD) is a very effective analytical technique commonly utilized for detecting and characterizing crystalline materials, such as iron oxide, as investigated in this study.

Identifying a successful iron oxide coating is commonly achieved by observing distinct peak positions indicative of various kinds of iron oxide. Each of the three main types of iron oxide, namely, hematite ( $\text{Fe}_2\text{O}_3$ ), magnetite ( $\text{Fe}_3\text{O}_4$ ), and wüstite ( $\text{FeO}$ ), display a unique XRD pattern. As an illustration, it is observed that hematite has a distinct diffraction peak at a  $2\theta$  value of roughly  $33.2^\circ$ , magnetite demonstrates a peak at approximately  $35.5^\circ$ , and wüstite is noted at around  $33^\circ$ . Interestingly, what implications might exist if the XRD

pattern of the glass beads exhibits peaks that align with particular  $2\theta$  values? This indicates the presence of certain specific forms of iron oxide. Moreover, the comparative magnitudes of these peaks might provide valuable information regarding the abundance or density of each component present in the specimen.

On the other hand, the XRD pattern obtained from uncoated glass beads predominantly exhibits the crystal structure inherent to the glass beads. Due to their amorphous or non-crystalline nature, glasses lack the distinct diffraction peaks commonly associated with crystalline substances. In contrast, the XRD patterns of these individuals generally exhibit a significant peak.

Nevertheless, the XRD pattern of the glass beads experiences a modification when an iron oxide coating is applied. Additional peaks are observed in the XRD pattern, which can be attributed to the iron oxide phases.

Therefore, the main difference observed in the XRD patterns of the glass beads with and without a coating is the existence of specific peaks, which can be attributed to the presence of iron oxide in the coated samples. The finding above provides irrefutable evidence of the efficacy of the coating process.

In addition, an in-depth examination of the XRD pattern was performed to determine the precise nature of the iron oxide species found in the glass beads with a coating. The observed peaks in our XRD pattern strongly correlate with the distinctive peaks associated with  $\alpha$   $\text{Fe}_2\text{O}_3$ , commonly known as hematite.

Figure 3 illustrates the X-ray diffraction analysis of the glass bead surfaces before and after applying the nano-iron coating. Significantly, the diffraction pattern observed from the coated glass beads at an angle of 25 thetas demonstrates a phase change at 0.12. The validation of the iron oxide deposited on the surface as  $\alpha$   $\text{Fe}_2\text{O}_3$  is supported by comparing these findings with a reference source [32]. Furthermore, the level of intensity observed on the glass surface undergoes an augmentation after applying the coating. This can be due to the enhanced crystalline structure of the surface, which results from the deposition of the nano-iron layers.

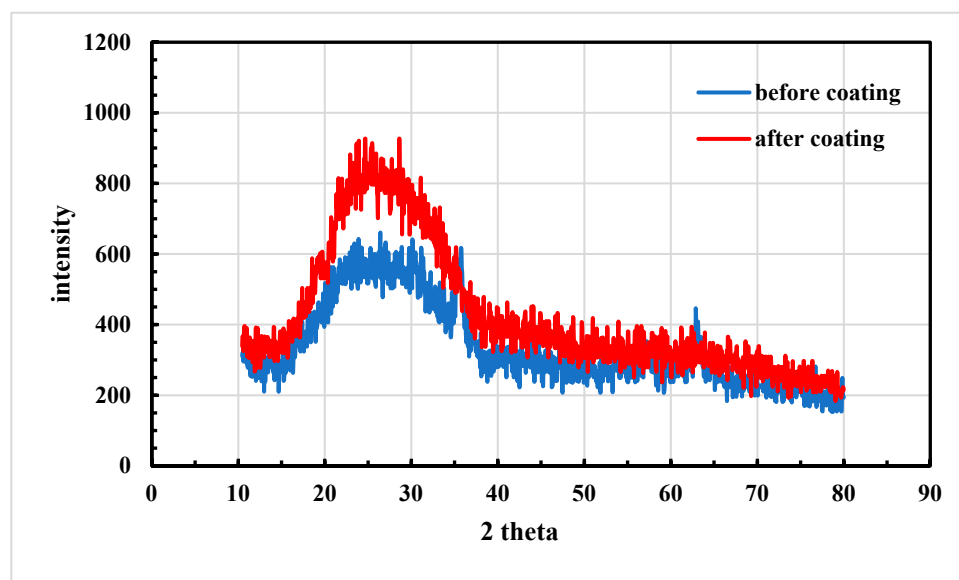


**Figure 3.** XRD patterns of coated glass beads before and after nano-iron coating.

### 3.2. The Influence of Coating on the Heat Transfer Characteristics of Glass Beads

Thermal diffusivity is an essential material characteristic that quantifies the speed at which thermal energy propagates inside a given material. Applying a thin layer over a material has the potential to modify the thermal diffusivity of the system, hence, exerting an influence on the overall thermal conductivity of the material. The equation  $k_{\text{eff}} = A + BT^3$  explains the phenomenon under consideration. In this equation,

$k_{\text{eff}}$  represents the effective thermal conductivity, which depends on the temperature (T). Coefficients A and B are included in the equation to account for the specific event characteristics [33].

The thermal conductivity of the glass bead surfaces before and after coating is presented in Table 3.

**Table 3.** Thermal conductivity of the glass bead surfaces pre- and post-coating.

T Heater Surface, °C	Thermal Conductivity before Coating, W/m. K	T Heater Surface, °C	Thermal Conductivity after Coating, W/m. K
98.7	0.00209615	101.5	0.002104568
85.6	0.002062722	90.3	0.002073631
75.9	0.002043725	78.5	0.002048374
66.7	0.002029674	68.4	0.002032001
61.8	0.002023603	62.4	0.002024297
57.9	0.00201941	59.6	0.002021171

The provided table presents data regarding the thermal conductivity of a gas–fluidized system, including glass beads, both before and after the iron oxide coating was applied. Thermal conductivity is a fundamental characteristic that indicates the capacity of a material to conduct heat, hence, playing a crucial part in determining heat transfer efficiency.

Although minimal, the observed increase in thermal conductivity after applying a coating significantly impacts heat transfer efficiency. The observed enhancement can be ascribed to the distinctive qualities of the iron oxide coating, which may have aided heat transfer by creating supplementary pathways for heat conduction or modifying the thermal properties of the bead surfaces.

It is important to mention that the heat transfer coefficients were measured under different operating conditions, and the fluidized bed operated under conditions of complete fluidization. It carefully monitored the system during experiments and observed that the glass beads were in continuous motion and fully fluidized.

After a more detailed analysis of the data was conducted, it became apparent that the impact of the coating on thermal conductivity becomes more noticeable at higher temperatures. The thermal conductivity of the coated glass beads demonstrates a more pronounced augmentation at elevated temperatures compared to the uncoated beads. This observation underscores the potential advantages of utilizing an iron oxide coating, mainly when elevated temperatures are widespread.

In summary, the data in the table provides more support for the efficacy of surface modification techniques, specifically coating, in enhancing heat transfer processes. The observed augmentation in thermal conductivity, particularly at elevated temperatures, indicates that an iron oxide coating benefits the heat transfer properties of glass beads in a fluidized system. The implications of these discoveries are significant for a range of applications, particularly in the context of fluidized bed systems, where the optimization of heat transmission is of paramount importance.

### 3.3. Influence of Air Superficial Velocity and Heating Power on Heat Transfer Coefficient before and after Coating

The effectiveness of heating power on the heat transfer coefficient was investigated in an air–glass bead fluidized bed. The study aimed to evaluate the impact of different heat inputs and velocities on the heat transfer coefficient before and after coating, as presented in Figures 4 and 5. The gas velocity and the power of the heater directly affect the heat transfer coefficient in a fluidized bed. An increase in gas velocity enhances the kinetic energy of particles, leading to better mixing and improved heat transfer. Similarly, a higher heater power provides more thermal energy, increasing the temperature gradient and driving heat transfer. However, it is crucial to maintain a balance to prevent hot spots and non-uniform heat distribution. In the industry, controlling these parameters is vital for processes

such as petroleum refining, waste treatment, chemical synthesis, and heat treatment of metals, as it allows for better process optimization, leading to improved efficiency and cost-effectiveness. The results show the heat transfer coefficient values before and after coating and operating a fluidized bed with heating using different heating fluxes and velocities. The values indicate an increased heat transfer coefficient after fluidized bed heating, which is more significant at higher velocities, as depicted in Figure 4. For instance, at a velocity of 0.106 m/s and a heating flux of 50 W, the heat transfer coefficient increased from 38.12 to 39.2 W/m<sup>2</sup>·°C after coating. At the same velocity but with a heating flux of 125 W, the heat transfer coefficient increased from 148.5 to 162.8 W/m<sup>2</sup>·°C after coating the glass beads, which represented a more significant increase.

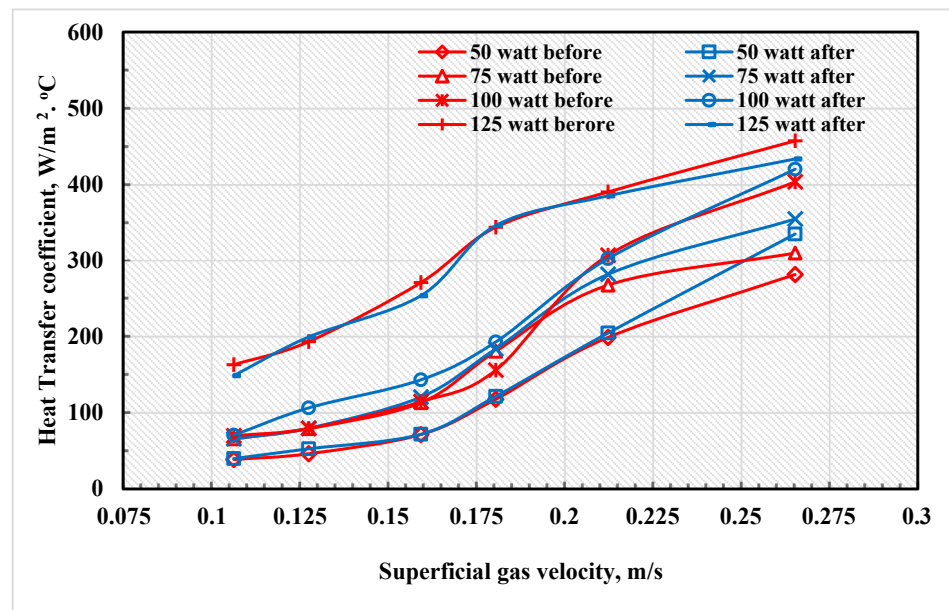


**Figure 4.** Impact of air superficial velocity on heat transfer coefficient at various heating powers for 200 µm glass beads before and after coating.

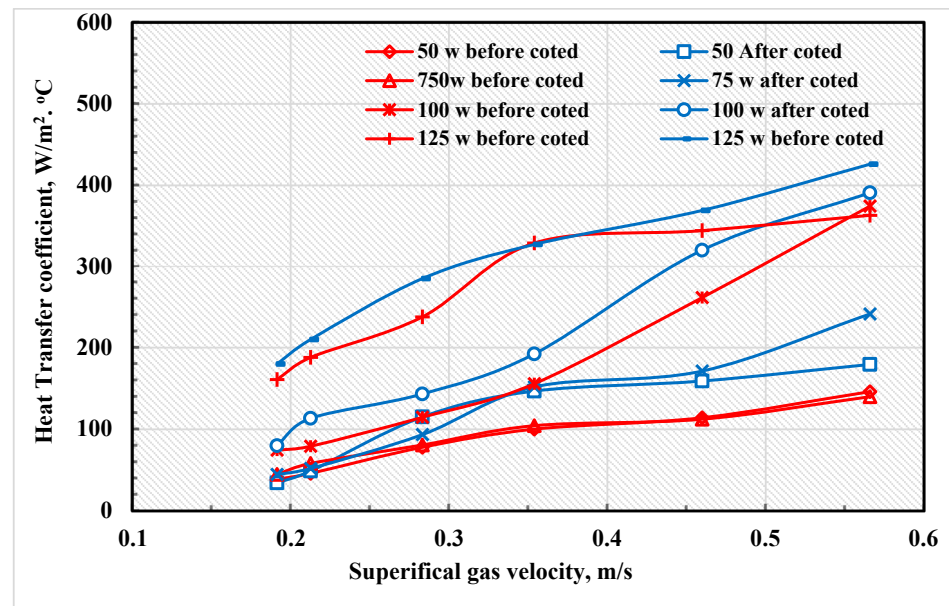


**Figure 5.** Influence of air superficial velocity on the heat transfer coefficient at various heating powers for 600 µm glass beads before and following coating.

Similarly, at a higher velocity of 0.27 m/s, the heat transfer coefficient increased from 281.6 to 334.9 W/m<sup>2</sup>·°C at a heating flux of 50 W and increased from 433.6 to 457.6 W/m<sup>2</sup>·°C at 125 W.

These results indicate that fluidized bed heating after coating can significantly enhance the heat transfer coefficient, and this enhancement is more significant at higher velocities. The findings suggest that fluidized bed heating with coated glass beads can be an effective process for heat transfer in industrial settings, particularly when higher velocities are used.

Figure 5 shows the results of a recent research study that investigated the effect of a heating flux in an air–glass beads fluidized bed on the heat transfer coefficient with different velocities. The study found that fluidized bed heating enhances the heat transfer coefficient, which is more significant at higher velocities and heating flux. For instance, at a velocity of 0.107 m/s and a heating flux of 50 W, the heat transfer coefficient increased from 40.7 to 42.1 W/m<sup>2</sup>·°C. At the same velocity but with a heating flux of 125, the heat transfer coefficient increased from 57.2 to 66.2 W/m<sup>2</sup>·°C, which represented a more significant increase. Moreover, at a higher velocity of 0.27 m/s, the heat transfer coefficient increased from 121.5 to 180.2 W/m<sup>2</sup>·°C at a heating flux of 50 W and from 336.4 to 390.3 W/m<sup>2</sup>·°C at 125 W. These results show that higher velocities and a higher heating flux can further enhance the heat transfer coefficient, indicating that fluidized bed heating can effectively transfer heat in industrial settings.

The observed increase in the heat transfer coefficient in a fluidized bed heating process, both before and after coating application, can be primarily attributed to two interconnected phenomena—conduction and convection. The operating parameters of velocity and heating power drive these phenomena. The high gas velocities give better fluidization and particle mixing, enhancing the convective heat transfer in the system. Increased gas velocity enhances the suspension and agitation of the glass beads within the fluidized bed, which promotes an overall higher heat transfer rate. This mechanism explains why an increased velocity resulted in a more significant enhancement of the heat transfer coefficient. Simultaneously, higher heating power provides more thermal energy to the system, driving the conduction process. The supplied heat spreads across the fluidized bed via the motion of particles and direct contact, creating a more significant temperature gradient and, thus, leading to a higher heat transfer coefficient. The more significant increase in the heat transfer coefficient at a heating flux of 125 W compared to 50 W can be attributed to this mechanism.

For example, at a superficial gas velocity of 0.106 m/s and a heating flux of 50 W, the heat transfer coefficient increased from 38.12 to 39.2 W/m<sup>2</sup>·°C after coating. This amounts to an increase of around 2.82%. Similarly, when subjected to an identical velocity but with a heating flux of 125 W, the heat transfer coefficient increased from 148.5 to 162.8 W/m<sup>2</sup>·°C after applying a coating, which signifies a 9.63% increase. These results indicate that the coating on the glass beads significantly enhanced the heat transfer coefficient, with percentage enhancements ranging from approximately 2.82% to 9.63%, depending on the specific operating conditions.

Applying a coating on the glass beads introduces another layer of complexity. The coating alters the surface properties of the bead, such as its thermal conductivity, emissivity, and surface area, which could lead to improved heat transfer. The coated beads showed a more significant increase in the heat transfer coefficient, emphasizing the role of the coating process in enhancing the heat transfer capabilities of the bed. The findings in their study showed that using certain materials could significantly enhance the heat transfer coefficient.

### 3.4. The Formulation of a Heat Transfer Correlation for Fluidized Beds

Several aspects of fluid dynamics within the bed influence the heat transfer coefficient correlation, including form, gas distributor design, and particle size distribution. Historically, researchers have commonly utilized the outcomes of prior experiments to develop correlations for heat transport in fluidized beds [34].

The present study has effectively formulated a heat transfer correlation specifically designed for fluidized beds. The correlation was established using specialist software, such as LABFIT, to analyze experimental data and obtain the aforementioned correlations.

The correlation mentioned above, derived from empirical data and established model parameters, can be expressed as follows:

$$Nu = 23 Re^{0.467} Pr^{3.242} \quad (3)$$

the equation above serves as a representation of the interdependence among the Nusselt number ( $Nu$ ), Reynolds number ( $Re$ ), and Prandtl number ( $Pr$ ) in the context of heat transfer occurring within the fluidized beds. The findings of our research endeavor to yield significant insights into the heat transfer characteristics shown by fluidized systems.

According to the data presented in Figure 6, there is a notable 5% disparity between the experimental and correlation models. In the existing body of literature on heat transmission in fluidized beds, many correlations have been established and characterized by the functional relationship  $Nu = (Re, r)$ .

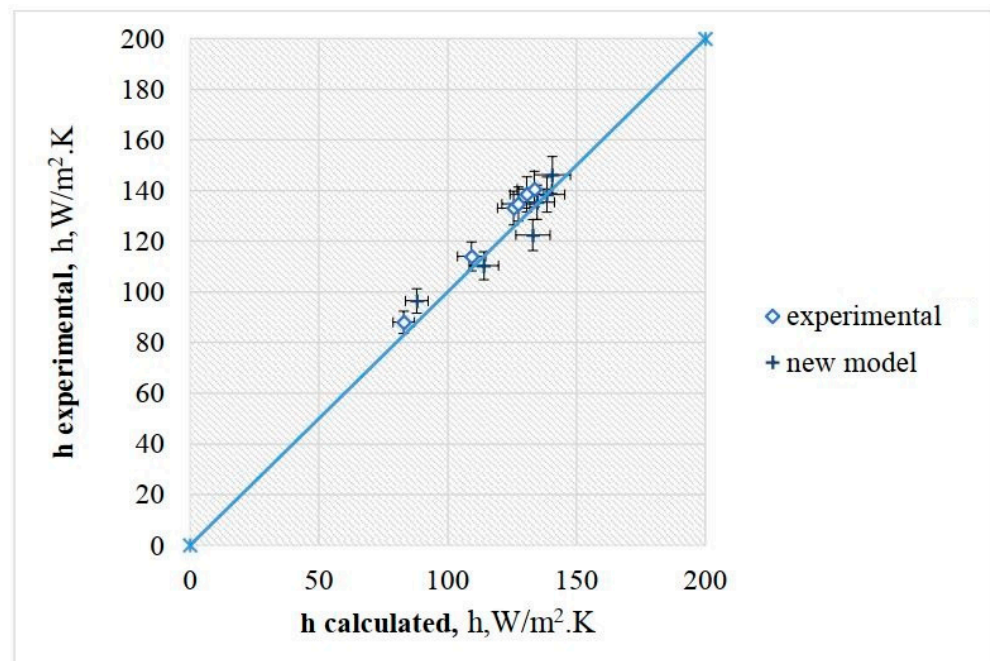
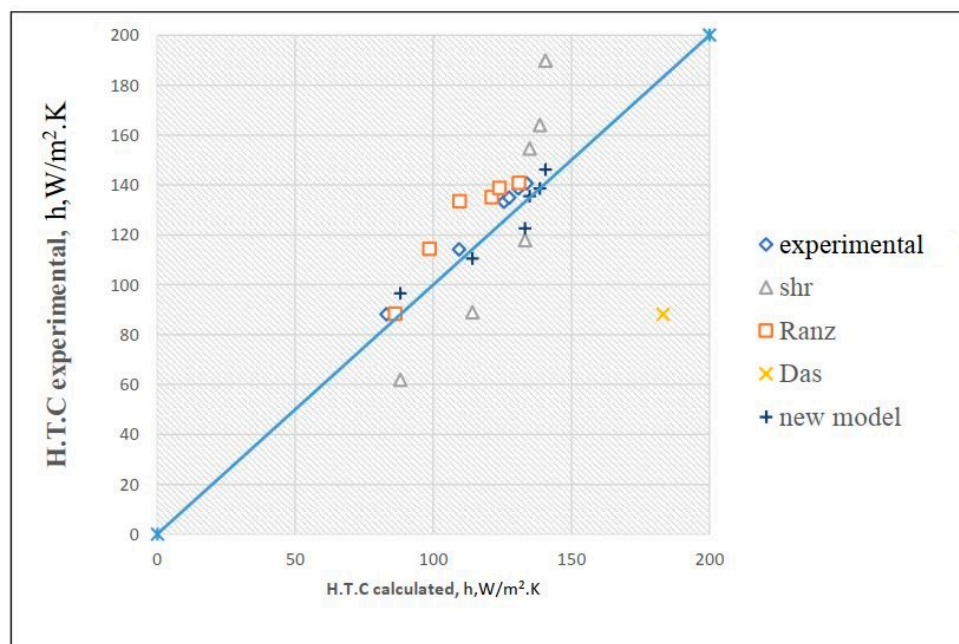


Figure 6. Comparison of experimental data with suggested correlation results.

Table 4 presents a comprehensive compilation of chosen correlations developed to predict the heat transfer coefficient in the fluidized bed column. Figure 7 illustrates a comparative analysis between the correlation that has been developed and a range of selected correlations. Figure 7 provides evidence that Ranz's correlation demonstrates a more robust correspondence with the data obtained from this particular investigation.

Table 4. Selected correlations for predicting heat transfer coefficient for fluidized bed.

Researcher	Conditions	Correlations
Ranz-Marshall [35]	$100 < Re < 1000$	$Nu = 2 + 1.8Re^{0.5}Pr^{0.33}$
Shrshab [36]		$Nu_p = 0.0268(Re_p)^{1.26} (Pr)^{0.48} (ks/kg)^{-0.0375} (1 - e/e)^{-0.173}$
Das [37]	$0 < Re < 500$	$Nu = (8.357.4e)(1 - 0.11Re^{0.2}Pr^{0.33}) + (3.92 - 7.67e + 3.96e^2) Re^{0.7} Pr^{0.33}$
Correlation with current study	$250 < Re < 700$	$Nu = 23 Re^{0.467} Pr^{3.242}$



**Figure 7.** Comparison between experimental data and selected correlations for predicting heat transfer coefficient for fluidized bed columns.

In general, the model yields reasonably accurate estimations for the heat transfer coefficients, considering the underlying assumptions and the straightforwardness of the model equation. The model provides estimations of the heat transfer coefficients with the computed values, encompassing all three particle sizes. Nevertheless, the observed percentage variations are conservative, from 1% to 10%. This implies that the current correlation reasonably accurately estimates the heat transfer coefficients under specific experimental conditions.

#### 4. Conclusions

This work thoroughly investigates the impact of iron oxide coatings on glass beads in fluidized bed systems, explicitly examining their potential to promote heat transfer. The study involved the characterization of the coated glass beads, examining the impact of air superficial velocity and heating power on heat transfer coefficients, and utilizing computational fluid dynamics (CFD) to understand the intricate temperature distributions within fluidized beds. Based on the findings of this study, it is possible to derive the following conclusions:

1. Iron oxide coatings led to a notable augmentation in the surface area of glass beads, as demonstrated by examining BET surface area. There was an observed increase in surface area from  $1.3801 \text{ m}^2/\text{g}$  to  $3.0511 \text{ m}^2/\text{g}$  following the coating process.
2. Scanning electron microscopy facilitated the observation of iron oxide crystalline structures on the surfaces of the coated glass beads. These iron oxide crystals exhibited an average diameter of 27 nm.
3. The presence of alpha  $\text{Fe}_2\text{O}_3$  on the surfaces of the glass beads after coating was verified through the analysis of X-ray diffraction patterns.
4. Applying a coating to the glass beads resulted in discernible enhancements in heat transfer coefficients. As an example, when the velocity was 0.27 m/s, and the heating flux was 125 W, the heat transfer coefficient for 600  $\mu\text{m}$  glass beads rose from  $336.4 \text{ W}/\text{m}^2\cdot\text{K}$  to  $390.3 \text{ W}/\text{m}^2\cdot\text{K}$ .
5. The heat transfer coefficients of the coated glass beads showed more pronounced improvements at elevated velocities and heating fluxes, suggesting efficacy in the coating, particularly in challenging industrial environments.

In conclusion, our thorough examination elucidates the notable advantages of iron oxide coatings in augmenting the heat transfer characteristics inside fluidized bed systems. The results provided in this study highlight the significant potential for achieving improved efficiency in industrial applications, particularly in scenarios characterized by higher velocities and heating fluxes. The quantitative insights provided offer a robust basis for industrial optimization and implementing sustainable practices.

**Author Contributions:** Conceptualization, J.M.A. and S.T.N.; methodology, F.H.F.; software, F.H.F.; validation, F.H.F.; formal analysis, F.H.F. and S.M.A.; investigation, F.H.F. and S.M.A.; resources, H.S.M.; data curation, F.H.F. and A.J.S.; writing—original draft preparation, F.H.F. and A.J.S.; writing—review and editing, A.J.S.; visualization, F.H.F. and S.M.A.; supervision, J.M.A. and S.T.N.; project administration, F.H.F. All authors have read and agreed to the published version of the manuscript.

**Funding:** This research received no external funding.

**Data Availability Statement:** The datasets generated during the current study will be available after publication.

**Acknowledgments:** The authors sincerely thank the University of Technology-Iraq and Al-Mustaqbal University for their invaluable support and resources.

**Conflicts of Interest:** The authors declare no conflict of interest.

## References

1. Yang, X.; Wang, S.; He, Y. Review of catalytic reforming for hydrogen production in a membrane-assisted fluidized bed reactor. *Renew. Sustain. Energy Rev.* **2022**, *154*, 111832. [\[CrossRef\]](#)
2. Gai, H.; Yang, P.; Zhang, Q.; Lin, M.; Song, H.; Xiao, M.; Huang, T.; Zhu, Q. Dual-dense gas-solid circulating fluidized bed reactor. *Fuel* **2023**, *337*, 126872. [\[CrossRef\]](#)
3. Du, S.; Wang, J.; Yu, Y.; Zhou, Q. Coarse-grained CFD-DEM simulation of coal and biomass co-gasification process in a fluidized bed reactor: Effects of particle size distribution and operating pressure. *Renew. Energy* **2023**, *202*, 483–498. [\[CrossRef\]](#)
4. Seckler, M.M. Crystallization in Fluidized Bed Reactors: From Fundamental Knowledge to Full-Scale Applications. *Crystals* **2022**, *12*, 1541. [\[CrossRef\]](#)
5. Tregambi, C.; Bevilacqua, C.; Troiano, M.; Solimene, R.; Salatino, P. A novel autothermal fluidized bed reactor for concentrated solar thermal applications. *Chem. Eng. J.* **2020**, *398*, 125702. [\[CrossRef\]](#)
6. Sabri, L.S.; Sultan, A.J.; Ali, J.M.; Majdi, H.S.; Al-Dahhan, M.H. Enhancing Heat Transfer Performance in Simulated Fischer–Tropsch Fluidized Bed Reactor through Tubes Ends Modifications. *ChemEngineering* **2023**, *7*, 85. [\[CrossRef\]](#)
7. Lee, J.M.; Lim, E.W.C. Heat transfer in a pulsating turbulent fluidized bed. *Appl. Therm. Eng.* **2020**, *174*, 115321. [\[CrossRef\]](#)
8. Wanchan, W.; Khongprom, P.; Limtrakul, S. Study of wall-to-bed heat transfer in circulating fluidized bed riser based on CFD simulation. *Chem. Eng. Res. Des.* **2020**, *156*, 442–455. [\[CrossRef\]](#)
9. Garcia-Gutierrez, L.M.; Hernández-Jiménez, F.; Cano-Pleite, E.; Soria-Verdugo, A. Experimental evaluation of the convection heat transfer coefficient of large particles moving freely in a fluidized bed reactor. *Int. J. Heat Mass Transf.* **2020**, *153*, 119612. [\[CrossRef\]](#)
10. Wu, Q.; Wang, S.; Zhang, K.; He, Y. Assessment of heat transfer performance in a swirling fluidized bed with binary mixture. *Appl. Therm. Eng.* **2021**, *194*, 117128. [\[CrossRef\]](#)
11. Tawfik, M.H.M.; Diab, M.R.; Abdelmotalib, H.M. Heat transfer and hydrodynamics of particles mixture in swirling fluidized bed. *Int. J. Therm. Sci.* **2020**, *147*, 106134. [\[CrossRef\]](#)
12. Bai, Y.; Qi, J.; Si, H. Analytical study on the Heat-Transfer Characteristics of a Fluidized Bed Reactor Heated by Multi-Stage Resistance. *Chem. Eng. Process.-Process Intensif.* **2021**, *164*, 108395. [\[CrossRef\]](#)
13. Hasan, Z.W.; Sultan, A.J.; Sabri, L.S.; Ali, J.M.; Salih, H.G.; Majdi, H.S.; Al-Dahhan, M.H. Experimental investigation on the impact of tube bundle designs on heat transfer coefficient in gas-solid fluidized bed reactor for Fischer–Tropsch synthesis. *Int. Commun. Heat Mass Transf.* **2022**, *136*, 106169. [\[CrossRef\]](#)
14. Abdulrahman, A.A.; Mahdy, O.S.; Sabri, L.S.; Sultan, A.J.; Al-Naseri, H.; Hasan, Z.W.; Majdi, H.S.; Ali, J.M. Experimental Investigation and Computational Fluid Dynamic Simulation of Hydrodynamics of Liquid–Solid Fluidized Beds. *ChemEngineering* **2022**, *6*, 37. [\[CrossRef\]](#)
15. Hasan, Z.W.; Sultan, A.J.; Tariq, M.; Sabri, L.S.; Salih, H.G.; Ali, J.M.; Al-Dahhan, M.H. Experimental investigation on heat transfer in a gas-solid fluidized bed with a bundle of heat exchanging tubes. *Eng. Technol. J.* **2022**, *40*, 1105–1116. [\[CrossRef\]](#)
16. Yang, M.; Jiang, F.; Qi, G.P.; Li, X.L. Heat transfer performance of a vapor–liquid–solid three-phase circulating fluidized bed evaporation system with different concentrations of Na<sub>2</sub>SO<sub>4</sub> solutions. *Appl. Therm. Eng.* **2020**, *180*, 115833. [\[CrossRef\]](#)
17. Hussein, A.T.; Abedalh, A.S.; Alomar, O.R. Enhancement performance of vapor compression system using nano copper oxide lubricant inside compressor and a fluidized bed for condenser cooling. *Case Stud. Therm. Eng.* **2023**, *44*, 102819. [\[CrossRef\]](#)

18. Krzywanski, J.; Grabowska, K.; Sosnowski, M.; Zylka, A.; Kulakowska, A.; Czakiert, T.; Sztékler, K.; Wesolowska, M.; Nowak, W. Heat Transfer in Adsorption Chillers with Fluidized Beds of Silica Gel, Zeolite, and Carbon Nanotubes. *Heat Transf. Eng.* **2022**, *43*, 172–182. [[CrossRef](#)]
19. Kasaeian, A.; Azarian, R.D.; Mahian, O.; Kolsi, L.; Chamkha, A.J.; Wongwises, S.; Pop, I. Nanofluid flow and heat transfer in porous media: A review of the latest developments. *Int. J. Heat Mass Transf.* **2017**, *107*, 778–791. [[CrossRef](#)]
20. Alsabery, A.I.; Abosinnee, A.S.; Al-Hadraawy, S.K.; Ismael, M.A.; Fteiti, M.A.; Hashim, I.; Sheremet, M.; Ghalambaz, M.; Chamkha, A.J. Convection heat transfer in enclosures with inner bodies: A review on single and two-phase nanofluid models. *Renew. Sustain. Energy Rev.* **2023**, *183*, 113424. [[CrossRef](#)]
21. Tsai, D.C.; Chang, Z.C.; Kuo, B.H.; Chen, E.C.; Huang, Y.L.; Hsieh, T.J.; Shieu, F.S. Thermal stability and optical properties of low emissivity multilayer coatings for energy-saving applications. *Ceram. Int.* **2020**, *46*, 7991–7997. [[CrossRef](#)]
22. SN Ch Dattu, V.; Rao Roniki, V.; Reddy Prasad, P.; Raju Tupati, P.; Gayatri Devi, N.; Chavakula, R. Influence of Nano-Fe<sub>2</sub>O<sub>3</sub> concentration on thermal characteristics of the water based Nano-fluid. *Mater. Today Proc.* **2022**, *62*, 2392–2395. [[CrossRef](#)]
23. Assaf, Y.H.; Akroot, A.; Abdul Wahhab, H.A.; Talal, W.; Bdaiwi, M.; Nawaf, M.Y. Impact of Nano Additives in Heat Exchangers with Twisted Tapes and Rings to Increase Efficiency: A Review. *Sustainability* **2023**, *15*, 7867. [[CrossRef](#)]
24. Liu, Y.; Wang, N.; Ding, Y. Preparation and properties of composite phase change material based on solar heat storage system. *J. Energy Storage* **2021**, *40*, 102805. [[CrossRef](#)]
25. Rabizadeh, M.; Ehsani, M.H. Effect of heat treatment on optical, electrical and thermal properties of ZnO/Cu/ZnO thin films for energy-saving application. *Ceram. Int.* **2022**, *48*, 16108–16113. [[CrossRef](#)]
26. Ellahi, R. Recent trends in coatings and thin film: Modeling and application. *Coatings* **2020**, *10*, 777. [[CrossRef](#)]
27. Nguyen, D.H.; Ahn, H.S. A comprehensive review on micro/nanoscale surface modification techniques for heat transfer enhancement in heat exchanger. *Int. J. Heat Mass Transf.* **2021**, *178*, 121601. [[CrossRef](#)]
28. Parida, K.; Bark, H.; Lee, P.S. Emerging Thermal Technology Enabled Augmented Reality. *Adv. Funct. Mater.* **2021**, *31*, 2007952. [[CrossRef](#)]
29. Kumar, R.; Youssry, S.M.; Joanni, E.; Sahoo, S.; Kawamura, G.; Matsuda, A. Microwave-assisted synthesis of iron oxide homogeneously dispersed on reduced graphene oxide for high-performance supercapacitor electrodes. *J. Energy Storage* **2022**, *56*, 105896. [[CrossRef](#)]
30. Slimani, S.; Meneghini, C.; Abdolrahimi, M.; Talone, A.; Murillo, J.P.M.; Barucca, G.; Yaacoub, N.; Imperatori, P.; Illés, E.; Smari, M.; et al. Spinel iron oxide by the co-precipitation method: Effect of the reaction atmosphere. *Appl. Sci.* **2021**, *11*, 5433. [[CrossRef](#)]
31. Shukrie, A.; Anuar, S.; Oumer, A.N. Air Distributor Designs for Fluidized Bed Combustors: A Review. *Eng. Technol. Appl. Sci. Res.* **2016**, *6*, 1029–1034. [[CrossRef](#)]
32. Devi, H.S.; Boda, M.A.; Shah, M.A.; Parveen, S.; Wani, A.H. Green synthesis of iron oxide nanoparticles using *Platanus orientalis* leaf extract for antifungal activity. *Green Process. Synth.* **2019**, *8*, 38–45. [[CrossRef](#)]
33. Sakatani, N.; Ogawa, K.; Iijima, Y.; Honda, R.; Tanaka, S.; Science, A.; Agency, A.E. Thermal Conductivity of Glass Beads as A Model Material of Regolith. In Proceedings of the 43rd Lunar and Planetary Science Conference, Woodlands, TX, USA, 19–23 March 2012; p. 2000.
34. Bisognin, P.C.; Câmara Bastos, J.C.S.; Meier, H.F.; Padoin, N.; Soares, C. Influence of different parameters on the tube-to-bed heat transfer coefficient in a gas-solid fluidized bed heat exchanger. *Chem. Eng. Process.-Process Intensif.* **2020**, *147*, 107693. [[CrossRef](#)]
35. Feng, L.; Wu, Y.; Guo, H.; Hu, Z.; Zhang, S.; Zhou, H. Effect of fluctuation on heat transfer enhancement of a spherical particle. *Int. Commun. Heat Mass Transf.* **2022**, *133*, 105981. [[CrossRef](#)]
36. Shreshab, M.A.; Abdulaziz, Y.I. Determination of Heat Transfer Coefficients in Air-Solid Fluidized Bed. *IOP Conf. Ser. Mater. Sci. Eng.* **2020**, *928*, 022067. [[CrossRef](#)]
37. Kieckhefen, P.; Pietsch-Braune, S.; Heinrich, S. Product-Property Guided Scale-Up of a Fluidized Bed Spray Granulation Process Using the CFD-DEM Method. *Processes* **2022**, *10*, 1291. [[CrossRef](#)]

**Disclaimer/Publisher's Note:** The statements, opinions and data contained in all publications are solely those of the individual author(s) and contributor(s) and not of MDPI and/or the editor(s). MDPI and/or the editor(s) disclaim responsibility for any injury to people or property resulting from any ideas, methods, instructions or products referred to in the content.